*Int. J. Heat Mass Transfer.* Vol. 31, No. 10, pp. 2047–2062, 1988
Printed in Great Britain

0017–9310/88 $3.00 + 0.00


# Effects of a forced Couette flow during the controlled solidification of a pure metal

CHARLES VIVÈS
Université d'Avignon, Laboratoire de Magnétohydrodynamique, 33, rue Louis Pasteur, 84000 Avignon, France

(*Received* 15 *December* 1987 *and in final form* 10 *March* 1988)

**Abstract**—The role of mixed convection, caused by a forced Couette flow, during the directional solidification of tin in a toroidal mould is studied. The macrostructure of the solidified melt is examined and the metallurgical findings (crystal growth) connected with the heat and fluid flow measurements. The results are compared with those obtained with another type of rotating flow, driven by a stationary electromagnetic field and produced by an annular electromagnetic conduction pump. The angle of deflection of the columnar crystals is related to the mean velocity and the shear stress upon the melt–solid interface, as well as to the initial superheat.

## 1. INTRODUCTION

THE INFLUENCE of natural convection on the controlled solidification of metals and alloys in moulds has been particularly studied over the last two decades, for various thermal boundary conditions [1–5]. These investigations were principally based on temperature measurements and have revealed that free convection in the metal pool during solidification plays an important role on the rate of evacuation of superheat, on the shape and movement of the melt–solid interface and on the structure of the solidified melt [1–4]. Recently, Gau and Viskanta [5] have studied the effect of natural convection on solidification of pure gallium under gravitationally unstable situations (melting from below or solidification from above) and shown the appearance of Bénard convection cells and convection rolls, which have an important impact on the interface shape.

It is an established fact that the morphology of a growing crystal is strongly affected by the fluid flow in the bulk liquid. The fluid motion is generally provoked either by natural convection or mixed free and forced convection. It should be emphasized that the grain structure of a metal is of great importance, since many of its mechanical properties are directly related to the size, shape and distribution of the grains. For instance, several dynamic methods, producing a vigorous forced convection in the melt during freezing, lead to substantial grain refinement. In such processes heat and fluid flow are controlled by various externally applied forces. The methods primarily include the use of electromagnetic or mechanical stirring [6–14]. In contrast, the production of large single crystals is made possible when the natural convection is strongly damped by the application of a stationary magnetic field of sufficient strength [15–17].

The purpose of this work is to study the effect of a forced Couette flow during the solidification of a pure metal. Since the pioneering investigations of Couette [18], Mallock [19] and Taylor [20], this complicated subject has been extensively studied and an excellent review of existing experimental and numerical results was presented by Cognet [21]. The problem is made still more difficult here, on account of the increasing number of parameters (involving the thermal parameters), acting in such an experiment, which is not isothermal. Moreover, the superheat, the melt volume, the geometric and thermal boundary conditions and hence the heat and fluid flow phenomena, are unsteady during solidification. So, the goal has been restricted to the examination of the main hydrodynamic and thermal parameters, which could be directly connected with the crystal structure of the solidified melt.

The practical interest of this study lies first in the fact that, in order to refine the grain, forced rotating flows are sometimes used in industrial casting processes. These dynamic treatments can be obtained either by an electromagnetic technique using rotary induction motors [6, 9, 12], or mechanical stirring through rotation of the mould [12, 13]. The present investigation will show another attractive application consisting in the control of the direction of crystal growth, so as to obtain blade-shaped columnar crystals, for example. The directional freezing technique has been particularly applied to turbine blade manufacture [22–24]. Directional solidification promotes a texture, namely dendritic growth in a preferred direction and this columnar structure avoids transverse grain boundaries, which are an initiating point for creep failure.

Moreover, this work bearing on the mechanical stirring of the melt during freezing, has been supplemented by some remarks on a specific electromagnetically driven rotating flow, which lends itself more easily to the establishment of several experimental relationships between the crystal features (i.e.

## NOMENCLATURE

| | |
|---|---|
| $B_0$ | externally imposed magnetic field |
| $c$ | specific heat |
| $D$ | average diameter of the crystals |
| $g$ | gravity |
| $Gr$ | Grashof number, $g\beta\rho^2H^3\Delta T/\eta^2$ |
| $H$ | liquid metal height |
| $H/(R_e-R_i)$ | aspect ratio |
| $I_0$ | externally imposed direct current |
| $J_0$ | externally imposed current density |
| $k$ | thermal conductivity |
| $L_f$ | latent heat of fusion |
| $M$ | Hartmann number, $B_0H(\sigma/\eta)^{1/2}$ |
| $r$ | radial position |
| $r^*$ | dimensionless radial position, $(R_e-r)/R_e$ |
| $Re'$ | Reynolds number, $UH\rho/\eta$ |
| $R_e$ | outer radius of the crucible |
| $R_i$ | inner radius of the crucible (or average radius of the interface) |
| $R_\omega$ | Reynolds number of rotation, $R_e(R_e-R_i)\omega_e/\nu$ |
| $T_0$ | initial temperature of the bulk liquid |
| $T_f$ | melting point |
| $\Delta T$ | initial superheat |
| $t$ | time |
| $t^*$ | dimensionless time, $\nu t/(R_e-R_i)^2$ |
| $U_\theta$ | tangential velocity component, in steady state |
| $U_{\theta,t}$ | tangential velocity component, in transient state |
| $U_e$ | circumferential velocity of the outer cylinder |
| $U_\theta^*$ | dimensionless velocity in transient state, $U_{\theta,t}/U_\theta$ |
| $U'_\theta$ | dimensionless velocity in steady state, $U_\theta/U_e$ |
| $z$ | vertical position (from the mould bottom). |

Greek symbols

| | |
|---|---|
| $\beta$ | thermal expansion coefficient of liquid |
| $\eta$ | viscosity |
| $\mu$ | magnetic permeability |
| $\nu$ | kinematic viscosity |
| $\rho$ | density |
| $\sigma$ | electric conductivity of liquid |
| $\tau$ | shear stress on the melt–solid interface |
| $\phi$ | angle of inclination of columnar crystals |
| $\omega_e$ | angular velocity of the exterior cylinder. |

size and inclination of the dendrites) and the main hydrodynamic and thermal parameters.

It is important to note that the present investigation is the continuation of previous experiments [10, 17] which, in any case, were performed using the same mould and the same metal and under identical thermal conditions, namely, the same initial superheat and the same flow rate of cooling fluid. The essential interest of such arrangements was to permit the realization of a comprehensive and comparative study of the interactions between the hydrodynamic, thermal and crystal growth phenomena, which occur in typical examples of crystallization of a pure metal in the presence of natural, forced and damped convection.

## 2. EXPERIMENTAL APPARATUS AND PROCEDURE

The apparatus for experiments is shown in Fig. 1. This apparatus is a modification of the system already described in detail [10, 17] and used for studies concerning the effects of natural and electromagnetically

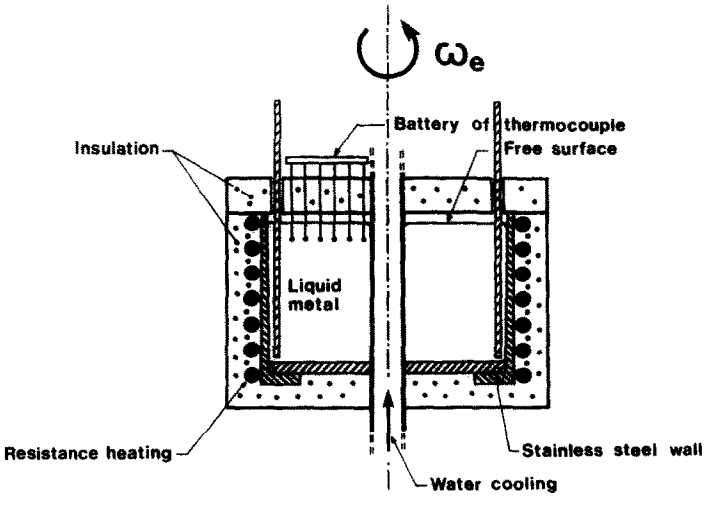


FIG. 1. Schematic diagram of the apparatus (Couette flow).

forced, or damped, convections during the solidification of a pure metal. In these previous investigations, the device consisted principally of an annular mould, made of stainless steel and containing about 2 $dm^3$ of a commercially pure tin (99.85% purity), with a free surface. The outer cylinder of 174 mm i.d. was resistance heated, while the inner cylinder of 24 mm o.d. was internally cooled by water at 20°C, with a flow rate of 1000 $dm^3\,h^{-1}$. All the exterior walls of the furnace were thermally insulated [10, 17].

The single modification consisted here in the supplementary presence of a rotating outer cylinder, with an interior diameter of 160 mm, driven with a constant angular velocity $\omega_e$ by an electric motor, through a pulley–belt system. A speed reduction gear permitted variations of $\omega_e$ ranging from 0 to 13.23 rad $s^{-1}$. Therefore, the molten metal was set in motion under the action of viscous forces caused by the rotation of the outer concentric cylinder, while the inner one was kept at rest.

The experimental procedure was the same as employed in the previous works [10, 17]. Temperature measurements were taken by means of a battery of six thermocouples, positioned horizontally along a radius, and likely to be placed at various prescribed heights within the melt. A six-channel recorder enabled evolution of the temperature distribution inside the bulk liquid with time during solidification to be followed (as well as the shape and position of the melt–solid interface). Each experiment was performed by melting the metal and heating it to 10°C above the required superheat temperature $T_0$, at this moment the heating was turned off in order that the liquid metal could cool slowly to $T_0$. Afterwards, the ingots were solidified by delivering cooling water from an initial superheat $\Delta T = T_0 - T_f$, above the melting point $T_f$.

Finally, prior to the examination of its macrostructure, each solidified specimen was sectioned, polished and macroetched [10, 17, 25].

## 3. VELOCITY MEASUREMENTS

It is difficult to carry out velocity measurements during a solidification, on account of the movement of the solidifying crust. So experimental runs have been performed without cooling, in order to avoid the solidification of the bath. The progression of the front, which results in a modification in time of the geometry of the annular pool, has been simulated by additional interior cylinders, of exterior radii $R_i$, and fashioned from solid stainless steel.

### 3.1. *Transient flow*

It is obviously essential here to know the time required to reach a fully developed flow. Consequently, the evolution of the tangential component of the local velocity with time has been recorded from the onset of the cylinder rotation, using an electromagnetic probe [26, 27], placed at a given point in the melt. Figure 2 shows two typical examples of recording, corresponding to different values of the rotation speed of the outer wall. The dimensionless parameter, $U_\theta^* = U_{\theta,t}/U_\theta$, represents the ratio of the tangential velocity component $U_{\theta,t}$, measured at a given time, to the $U_\theta$ component measured at the same point, in the steady state; $t^* = vt/(R_e - R_i)^2$ is an adimensional time.

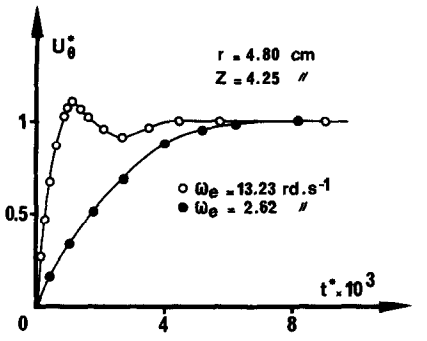


FIG. 2. Tangential velocity component measured in the transient state, at a given point and for two values of the angular velocity of the rotating cylinder.

It occurs that, when the cylinder rotates at a relatively low rate ($\omega_e = 2.62$ rad $s^{-1}$), the evolution of the azimuthal velocity component exhibits an exponential trend. For a higher rotation speed ($\omega_e = 13.23$ rad $s^{-1}$), it can be seen that $U_\theta^*$ increases rapidly, passes through a maximum and then decreases up to a minimum, from which the molten metal is once again accelerated and the steady state is finally reached. This phenomenon corresponds very probably to a transition state from laminar to turbulent flow. Moreover, it is seen that the fully developed flow is reached more rapidly as the angular velocity of the rotating cylinder is high. As an illustration, the steady Couette flow is nearly obtained after about 70 s, for $\omega_e = 13.23$ rad $s^{-1}$, and after about 140 s, for $\omega_e = 2.62$ rad $s^{-1}$.

### 3.2. *Steady flow*

3.2.1. *Tangential component.* Figure 3 presents the distribution of the adimensional parameter $U'_\theta =$

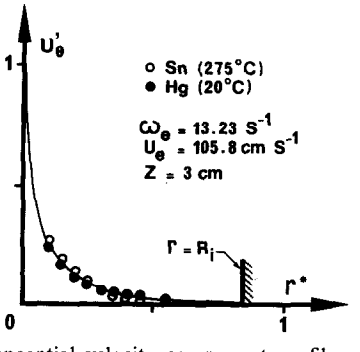


FIG. 3. Tangential velocity component profile, plotted in steady state.

$U_\theta/U_e$ (which is the ratio of the tangential component $U_\theta$ of the liquid velocity to the circumferential velocity of the rotating cylinder $U_e$) as a function of the radial position, defined by the dimensionless parameter $r^* = (R_e - r)/R_e$. It appears that, because of the low viscosity of the liquid metal, the azimuthal velocity decreases rapidly, from the rotating wall towards the centre of the melt. The fluid is practically unmoved inside a zone located between the inner cylinder and the mid-radius of the pool. Moreover, the kinematic similarity between mercury and tin flows can be satisfactorily observed. Furthermore, supplementary experiments have proven that these velocity profiles are practically independent of the vertical position except, obviously, in the vicinity of the horizontal bottom wall.

3.2.2. *Secondary flow*. Methodical measurements, performed inside a radial cross-section of the melt, reveals the presence of a secondary flow (Fig. 4), with radial and axial velocity components. The flow pattern, presented in Fig. 4, presents some similarities with that produced by a strong natural convection, characterized by an ascending flow along the hot wall and a descending flow along the cold wall [10, 17]. This loop occurs for the values of the Reynolds number of rotation, $R_\omega = R_e(R_e - R_i)\omega_e/\nu$, ranging between $5.5 \times 10^4$ and $2.8 \times 10^5$. It is seen that the stirring intensity is more intense in the upper part of the melt than in the vicinity of the bottom, whereas the peak velocity, measured within this vortex exceeds 5 cm $s^{-1}$; hence, the stirring intensity can be here more important than in the main flow, except in the neighbourhood of the rotating wall.

It must be noted that, owing to the three-dimensional character of the fluid motion, the volumetric flow rate is not conserved inside such a cross-section. On the other hand, it has not been possible to explore completely the regions situated in the near proximity of the vertical walls, on account of a probe–wall interaction effect.

In the case of an isothermal Couette flow, it is established that, as a rule, when the outer cylinder rotates while the inner one is at rest, the centrifugal forces are irrotational and, consequently, balanced by a pressure gradient. So, in contrast to the inverse case (i.e. rotating inner cylinder and outer cylinder unmoved), any secondary flow is likely to appear, under these circumstances.

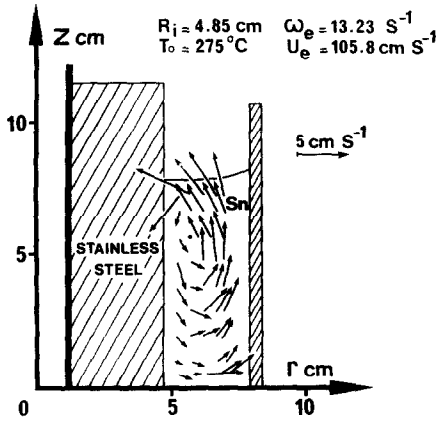


FIG. 4. Velocity pattern plotted inside a radial cross-section of the tin pool.

In the present system, the mechanism of the formation of this unexpected secondary flow has not been well understood and can perhaps be attributed to a bottom effect, caused by the horizontal wall of the crucible. Nevertheless, the presence of this cell was confirmed by repetitive tests and will be corroborated later by inspection of macrographies.

## 4. TEMPERATURE MEASUREMENTS

The isotherm maps obtained in natural convection (i.e. with no rotation), for various values of superheat, have already been presented [10, 17] and, consequently, are not reproduced here. Their inspections have mainly revealed the presence of a hot zone located in the vicinity of the free surface, while the radial and vertical thermal gradients are much steeper in the upper part than in the neighbourhood of the bottom of the solidifying melt.

Figure 5 shows the evolution of the temperature distribution plotted in the liquid metal pool during freezing, for an angular velocity of the outer cylinder $\omega_e$ of 13.23 rad $s^{-1}$ and an initial superheat of 43°C. Inspection of Figs. 5(a) and (b), connected with the early stages of solidification, reveals the existence of two different zones. Very steep horizontal and vertical thermal gradients appear along the interface in the upper left-hand corner of the cavity, while the thickness of the thermal boundary layer is found to increase downward along the solidifying crust. Moreover, the isotherms are nearly horizontal in the upper half and vertical in the lower half. The low thermal gradients, which exist in the bottom region indicate that conduction seems the preferential mechanism of heat transfer and that velocities are very probably smaller in this zone. On the other hand, the existence of a cell, filling about 3/4 of the volume occupied by the molten metal, can be anticipated. These expectations are in agreement with the remarks expressed after inspection of the secondary flow field, displayed in Fig. 4.

At the initiation of the liquid–solid phase change, the hotter zone is situated in the proximity of the free surface, and the difference between the extreme temperatures (i.e. from top to bottom) is 16°C, for $t = 50$ s (Fig. 5(a)), while the difference was 24°C in natural convection [10]. This observation is obviously explained by the fact that, with regard to the case of natural convection, the stirring, which is here largely provoked by the secondary flow, promotes a more rapid dissipation of superheat. For the same reason, the growing of the solidified portion is markedly slowed down in the upper part of the pool (Figs.

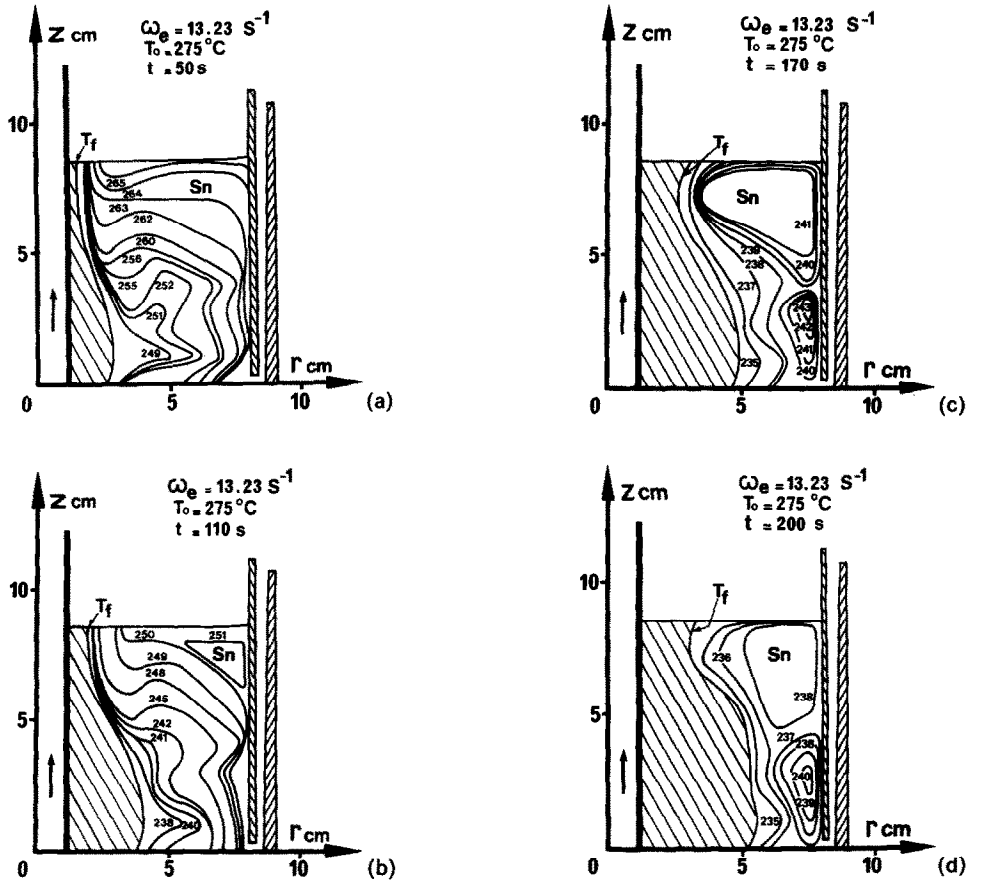


FIG. 5. Temperature fields plotted in the presence of a forced Couette flow ($\Delta T = 43°C$): (a) $t = 50$ s; (b) $t = 110$ s; (c) $t = 170$ s; (d) $t = 200$ s.

5(a) and (b)), because the liberation of latent heat is hindered on account of the higher intensity of the convective flow in this region.

In the course of solidification, the temperature of the melt tends to be uniformized under the action of mixed convection (Figs. 5(c) and (d)) and a very slightly hotter zone even occurs, in the bottom region. This later observation confirms the predominance of a convective mode of heat transfer in the upper region, and of a conductive mode in the lower zone. Inspection of these isotherm maps shows the probable presence of two vortices, the volume of the upper cell decreasing in favour of the lower loop during freezing. The existence of these loops, where the velocities are probably weak, may be understood by the evolution of the aspect ratio $H/(R_e - R_i)$, due to the advancement of the solidification front, of average radius $R_i$.

Temperature profiles plotted, either in natural convection, or in the presence of a forced Couette flow, are compared in Figs. 6 and 7. It should be mentioned that, under the present experimental conditions, the convective process corresponds rather to a mixed convection mode (the adimensional group $Gr/R'e^2$ is of the order of ten). For this reason, the discrepancy between the temperature distributions is not as pronounced as in the case of an efficient electromagnetic stirring caused, for instance, by the application of an induction electromagnetic field [10].

Temperature profiles, plotted along a radius, at different levels, are conveyed in Fig. 6. Their inspection shows that, in the upper half of the mould (Fig. 6(a)), the central region is isothermal in the horizontal direction and confirms that the temperatures are smaller in the case of the Couette flow, because the convective stirring is strengthened by the secondary flow (Fig. 4). Moreover, in the bottom area (Fig. 6(c)), the temperature tends roughly to a linear variation in the core region, due to the predominance of a radial conductive heat flux in this lower zone.

The profiles, conveyed in Fig. 7(a), have been plotted along a vertical approximately situated at mid-radius ($r = 4$ cm); it is seen that the temperature of the core region decreases almost linearly, from top to bottom. Figure 7(b) presents a temperature distribution corresponding to a vertical close to the external wall ($r = 7$ cm). In the case of the Couette flow, the more complicated shape of the temperature profile is probably due to the combined effect of the rotating flow (driven by the outer cylinder) and of the secondary loop. The temperature increases suddenly in

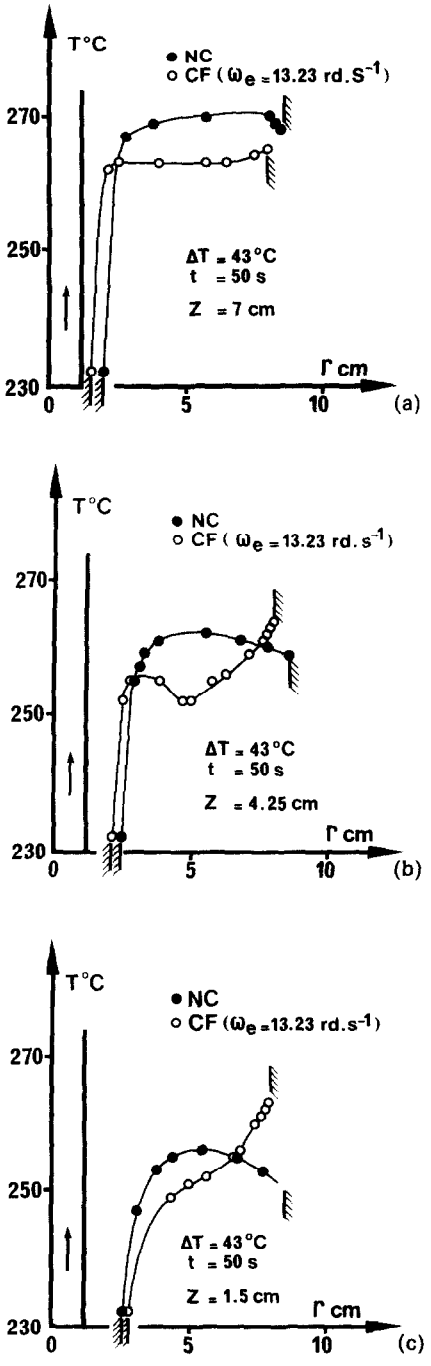


FIG. 6. Temperature profiles plotted along a radius in natural convection (NC) and in the presence of a forced Couette flow (CF): (a) $Z = 7$ cm; (b) $Z = 4.25$ cm; (c) $Z = 1.5$ cm.

the vicinity of the bottom of the crucible; this observation once again argues the case for weaker heat and mass transfer in this area.

Figure 8 displays the shape and position of the solid–liquid interface, drawn at a given time, in the absence and presence of forced rotation. It appears that, compared with the case of free convection, the average solidification rate is slowed down because the

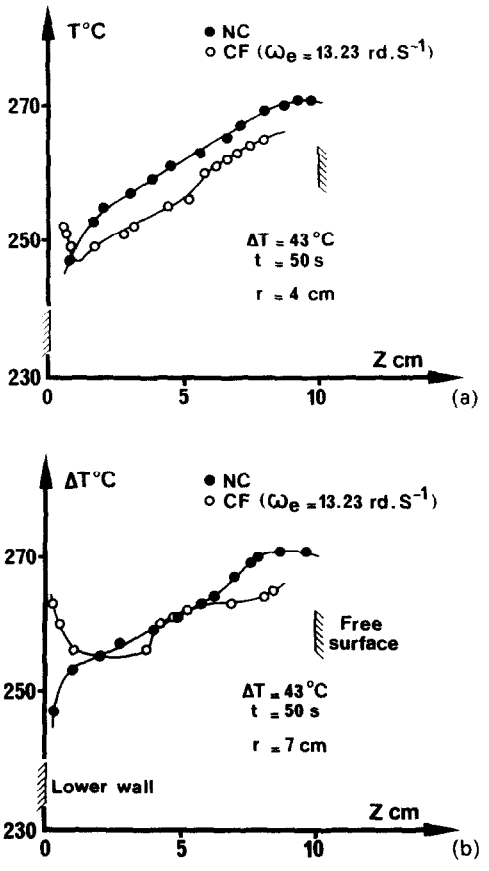


FIG. 7. Temperature profiles plotted along a vertical in natural convection (NC) and in the presence of a forced Couette flow (CF): (a) $r = 4$ cm; (b) $r = 7$ cm.

liberation of latent heat is delayed to the profit of the superheat drop (stirring effect). Moreover, in the presence of the Couette flow, the solidification front exhibits, in the top region, a concave shape which very probably coincides with the existence of the secondary vortex, already pointed out.

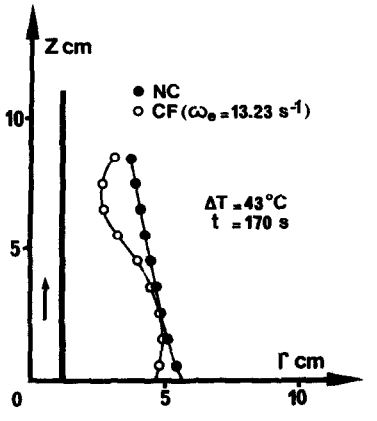


FIG. 8. Shape and position of the melt–solid interface in natural convection (NC) and in the presence of a forced Couette flow (CF).

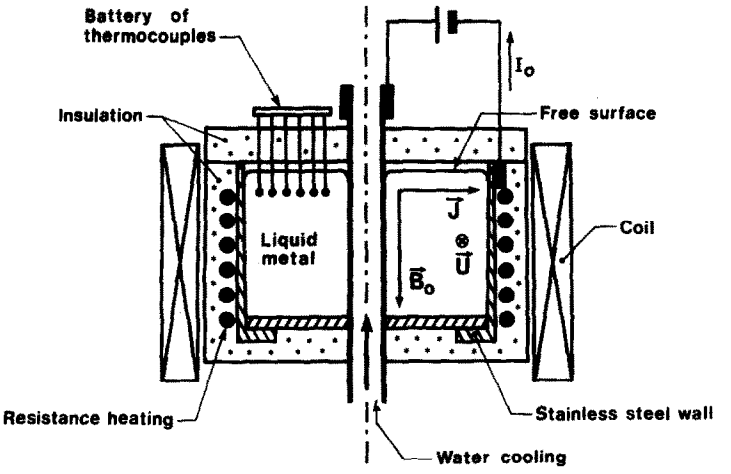


FIG. 9. Schematic diagram of the apparatus (electromagnetic rotation).

## 5. REMARKS ON AN ELECTROMAGNETICALLY DRIVEN ROTATING FLOW

During solidification, the tin pool was subjected both to an externally imposed axial and stationary magnetic field and to a radial electric field, giving rise to a tangential electromagnetic body force distribution, throughout the melt (Fig. 9). Hence, the system behaved as an annular electromagnetic conduction pump and the liquid metal was set in rotation under the action of the steady electromagnetic force pattern.

A magnetic field $B_0$, uniform to 2% inside the melt, was generated by an inductor made up of 248 jointed turns traversed by a direct current, liable to vary within the range of 0–165 A, whereas the corresponding strength $B_0$ was included between 0 and 0.1 T. Furthermore, a constant voltage was applied between the inner and outer cylinders of the crucible; these walls, playing the role of electrodes, permitted the flow of a radial direct current $I_0$ (between 0 and 250 A) through the solidifying metal to take place. In the case of the hydrodynamic study and in order to allow easier operation in the steady state, the progression of the solidification front has again been simulated by the adjunction of inner cylinders, made of stainless steel and of exterior radii $R_i$.

Preliminary experiments showed that a steady state rotation speed of the molten metal was reached after a transient time of about 30 s. The tangential velocity profiles presented in Fig. 10, were plotted along a radius, at mid-height of the melt and at different stages of solidification (i.e. for various simulated positions of the front of radius $R_i$). The Hartmann number $M$, which is proportional to the magnetic field $B_0$, has been already defined [17]. The inspection of these velocity distributions reveals the decay of the electromagnetically driven fluid flow inside the tin pool during freezing. This damping is caused both by the increasing surface area of the interface, which results

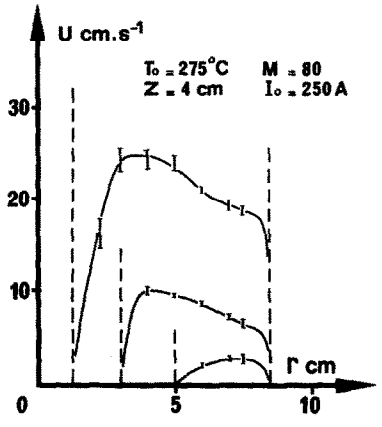


FIG. 10. Tangential velocity profiles, plotted for different positions of the solidifying crust.

in an enhancement of the viscous frictional forces, and by the decline of the externally imposed electromagnetic body force $\mathbf{J}_0 \times \mathbf{B}_0$, acting on a unit volume of the fluid. Indeed, $\mathbf{J}_0 \times \mathbf{B}_0$ is nonuniform; the forces decrease along a radius, from the inner cylinder to the outer one, on account of Kirchhoff's first law: $\operatorname{div} \mathbf{J}_0 = 0$.

Subsidiary experiments showed that, for a given radial position, the tangential velocity was practically independent of the vertical position, except in the near vicinity of the bottom of the mould (no slip condition) and of the liquid free surface. Moreover, a weak unicellular fluid motion (with measured velocity peaks of the order of 3 cm s$^{-1}$), mainly located in the upper half of the pool, has been detected inside a radial cross-section, at the onset of freezing.

Temperature measurements were again performed from an initial superheat of 43°C. The shape of the isotherms, sketched in Fig. 11, presents some similarities with those already seen in natural convection [10, 17]. Inspection of this isotherm map, plotted at the initiation of solidification, confirms the presence

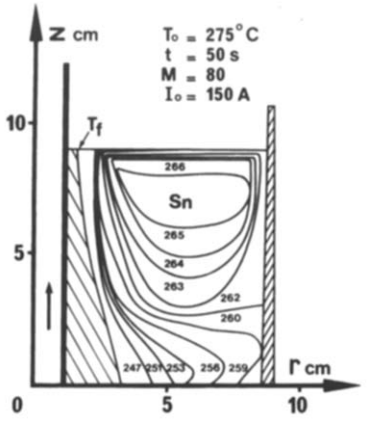


FIG. 11. Temperature field, plotted in the presence of crossed electric and magnetic fields.

of a single loop located in the upper part of the bath, while the low radial thermal gradients, seen in the bottom region, indicate the dominance of conduction in this latter zone.

## 6. CRYSTAL GROWTH AND DISCUSSION

### 6.1. *Natural convection*

The presence of a unicellular molten metal flow, with fluid rising near the hot wall and descending near the cold one, has been detected in a previous work [10]. It has also been shown that the columnar zone is sloped in the upstream direction to the interface [28, 29] and that the inclination of the dendrites increases with the degree of superheat (Fig. 12(a)), mainly at the onset of freezing. It should be noted that the left- and right-hand sides of the samples, presented in Fig. 12 and cut along the whole radial and vertical cross-sections of the toroidal ingots, are respectively connected with the cold and hot wall of the mould. Figure 13(a) shows a horizontal slice solidified from a low initial superheat of 3°C. Owing to the weakness of the free convection, the conductive and radial mode of heat transfer is here predominant; it follows that the crystal grows horizontally. Moreover, the radial crystal growing direction proves the absence of a tangential component of the melt. The sample presented in Fig. 13(b) relates to 43°C of superheat and displays the sections of the oblique columns, already seen in Fig. 12(a).

### 6.2. *Couette flow*

Figure 12(b) displays a specimen obtained from an initial superheat of 100°C and an angular velocity of 13.23 rad $s^{-1}$. It appears that the effect of the rotating outer cylinder results, for a given initial superheat, in a diminution of the average diameter of the columns


FIG. 12. Macrostructures of commercially pure tin (vertical slices) solidified in natural convection, (a) $\Delta T = 100°C$, in the presence of a forced Couette flow, (b) $\Delta T = 100°C$, $\omega_e = 13.23$ rad $s^{-1}$, and in the presence of crossed electric and magnetic fields, (c) $\Delta T = 100°C$, $M = 80$, $I_0 = 250$ A.

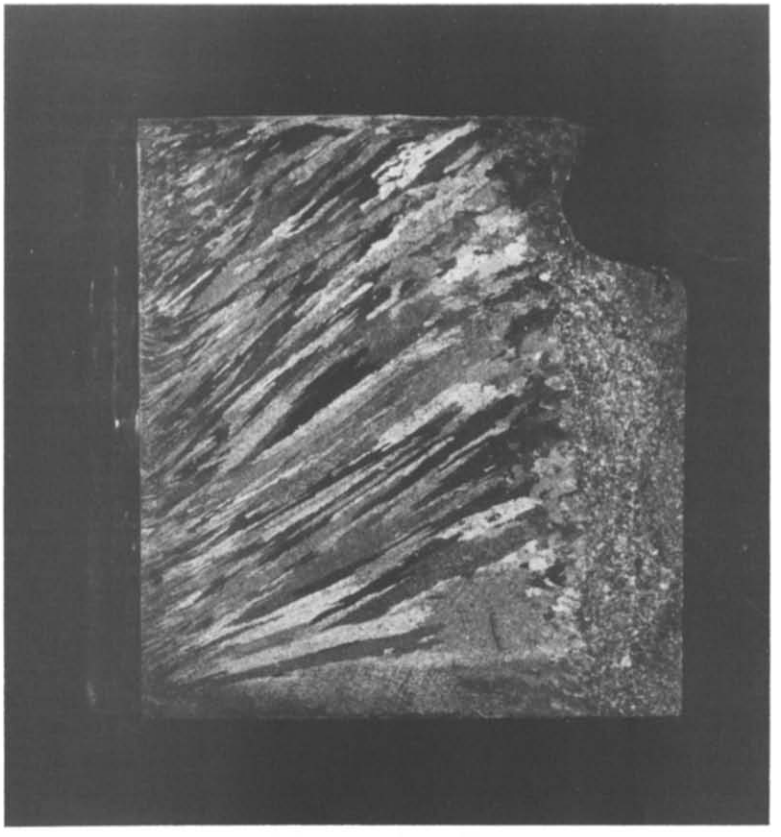

(b)

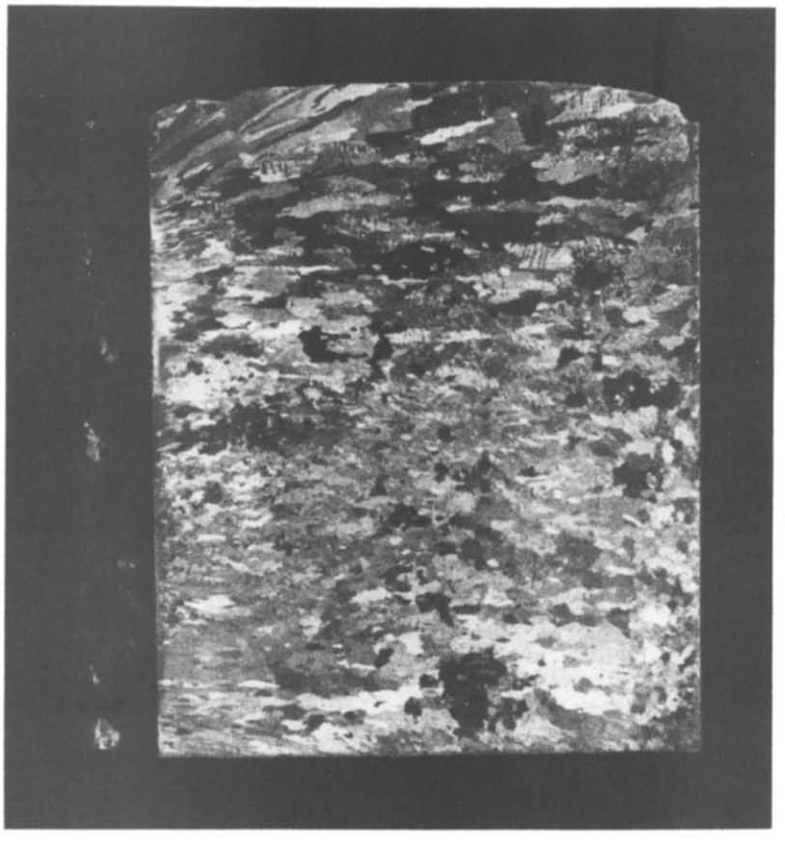

(c)

FIG. 12.—*Continued.*

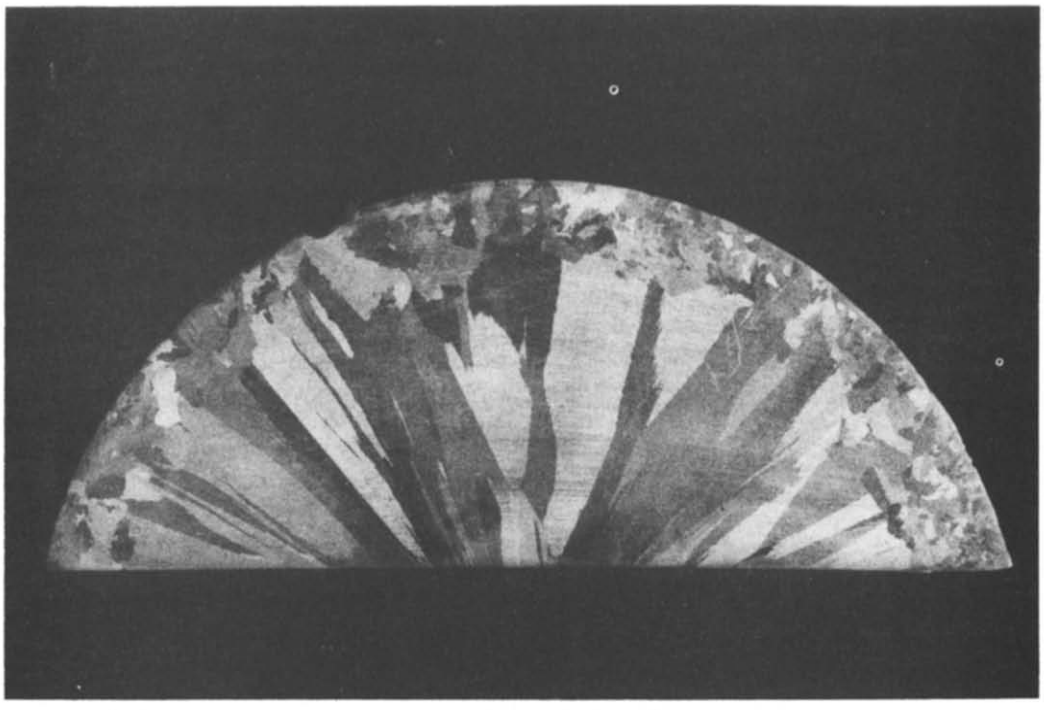

(a)

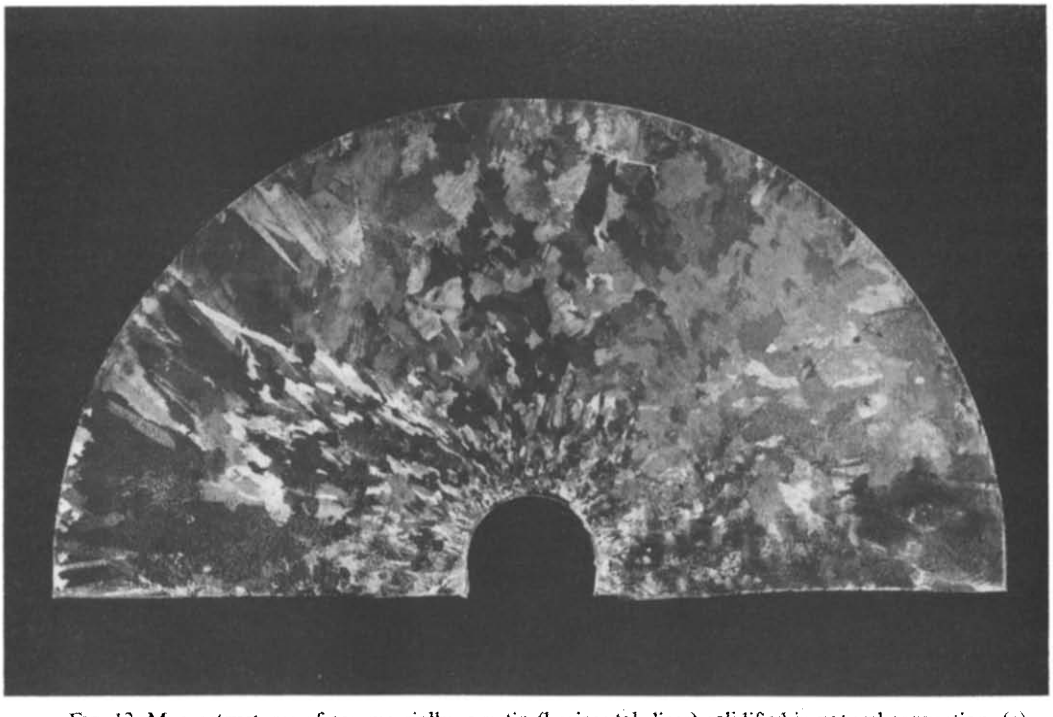

(b)

FIG. 13. Macrostructures of commercially pure tin (horizontal slices) solidified in natural convection, (a) $\Delta T = 3°C$, (b) $\Delta T = 43°C$, in the presence of a forced Couette flow, (c) $\Delta T = 43°C$, $\omega_e = 13.23$ rad $s^{-1}$, (d) $\Delta T = 100°C$, $\omega_e = 13.23$ rad $s^{-1}$ and in the presence of crossed electric and magnetic fields, (e) $\Delta T = 100°C$, $M = 80$, $I_0 = 250$ A, (f) $\Delta T = 100°C$, $M = 80$, $I_0 = 250$ A (periodic reversals of the flow rotation).

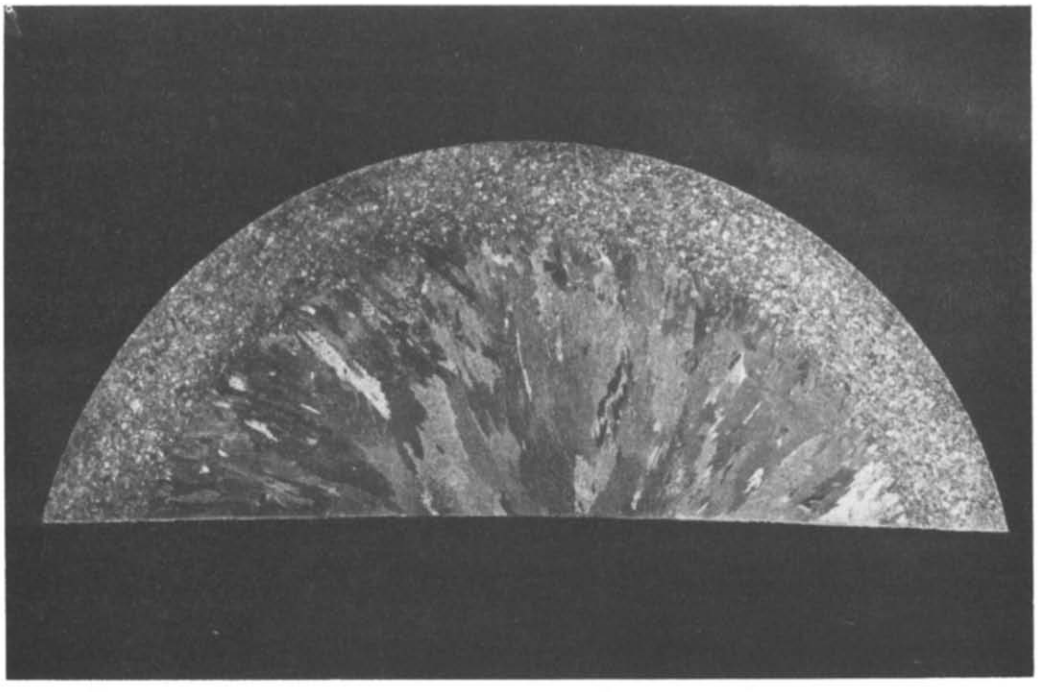

(c)

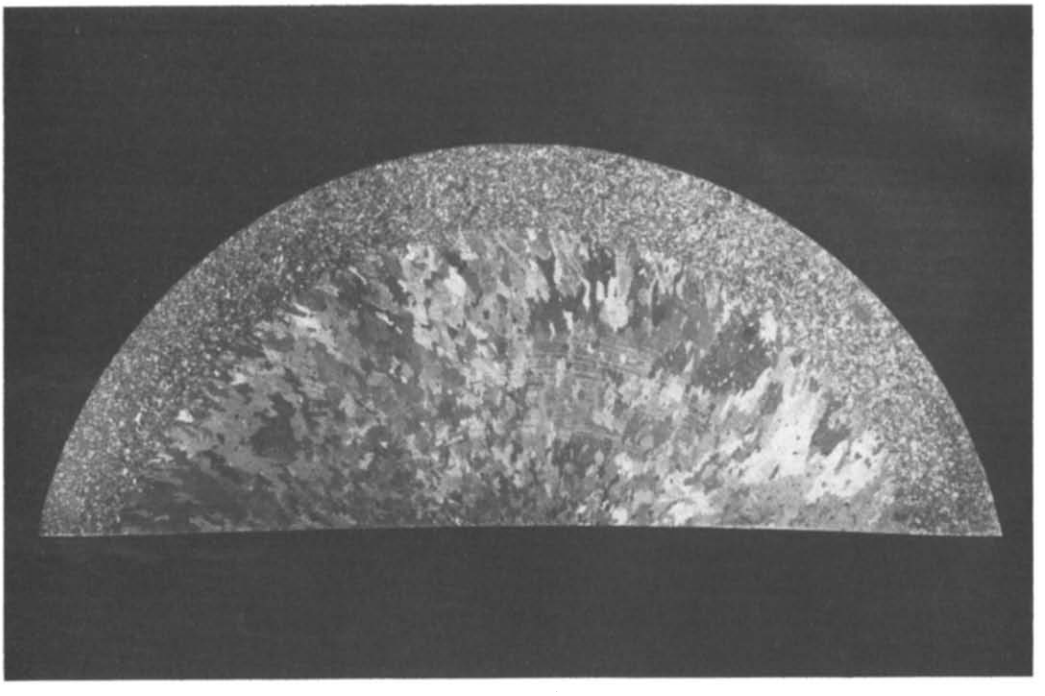

(d)

FIG. 13.—*Continued.*

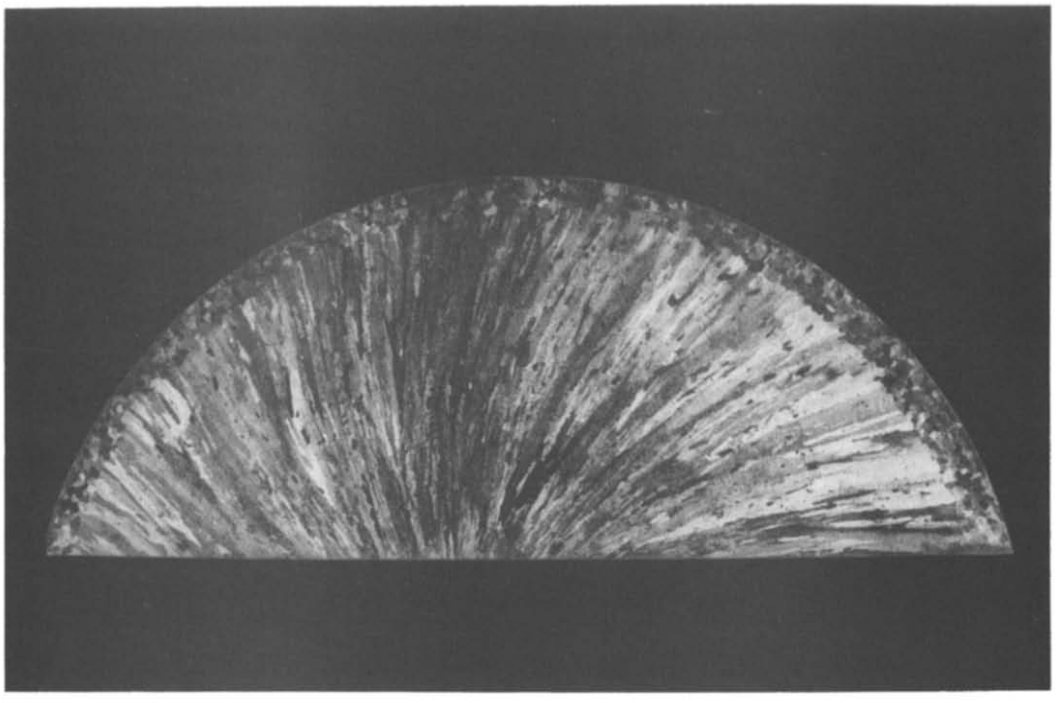

(e)

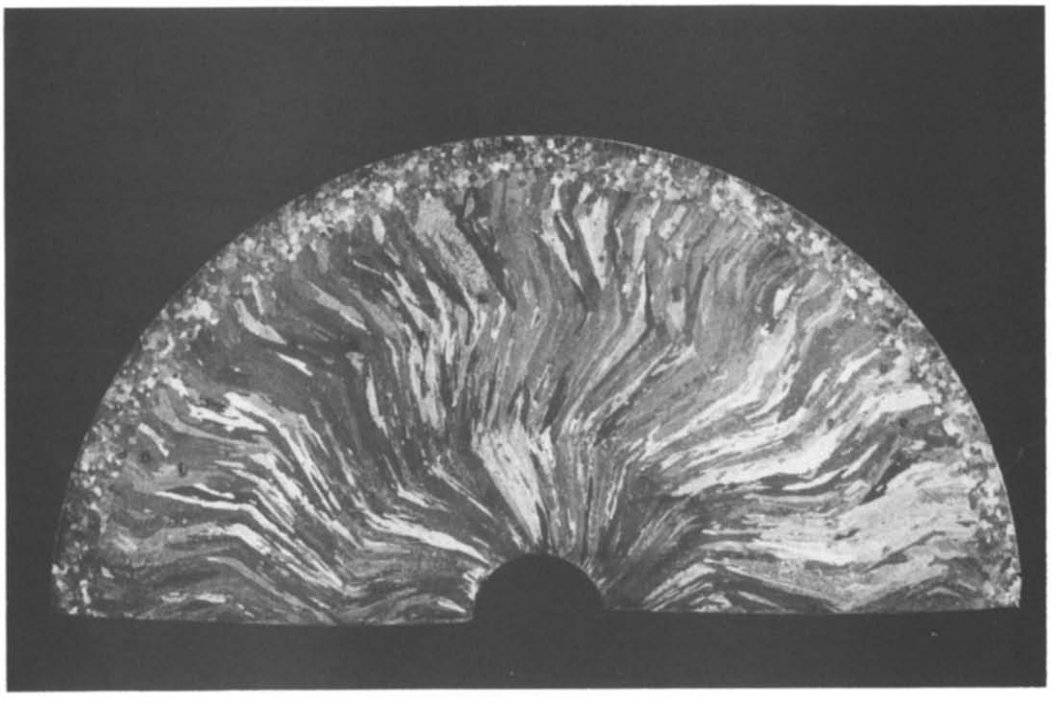

(f)

FIG. 13.—*Continued.*

and in an enhancement of their angle of inclination $\phi$. Obviously, the inclination of the dendrites is enhanced by the secondary vortex, pointed out in Fig. 4. Moreover, at the start of solidification, $\phi$ is greater in the upper part than in the lower region of the ingot; this finding is consistent with the comments expressed after examination of the flow structure, displayed in Fig. 4, and of the temperature distributions, depicted in Figs. 5(a) and (b). Figures 14(a) and (b) show that the deflection angle of the dendrites increases, while their average diameter decreases, when the initial superheat and the rotation speed of the outer cylinder increase.

On the other hand, a fine equiaxed structure (the diameter of the grains is included between the range 50–400 $\mu$m) is observed in the cortical zone (Figs. 12(b), 13(c) and (d)). This sudden and spectacular change of crystal structure is most likely provoked both by the superheat drop and the tangential liquid metal flow. Indeed, the multiplication of floating nuclei is favoured in the completion of solidification, because the temperature of the liquid metal pool is practically equal to the melting point (Fig. 17). Furthermore, during the latter stages of freezing, the rotation of the outer cylinder results in an increasing shear rate in the melt (caused by the augmentation of the tangential velocities in this area and by the reduction of the space between the solidifying crust and the external wall). It is well known that such conditions promote the production of very fine grained suspensions.

To summarize, it appears clearly that this outward solidification takes place successively from two very different mechanisms: the growing of the columnar macrostructure is mainly under the dependence of the secondary flow, while the production of the equiaxed crystals is only due to the main tangential flow.

Figures 13(c) and (d) exhibit two horizontal slices corresponding to an initial superheat of 43 and 100°C, respectively, and show again the sections of the deflected columns. A tendency to a slight inclination of the dendrites, caused by the weak tangential velocity of the fluid flow in the area of the columnar crystal growth, can be discerned. However, it is obvious that the effect of the secondary flow is here predominant.

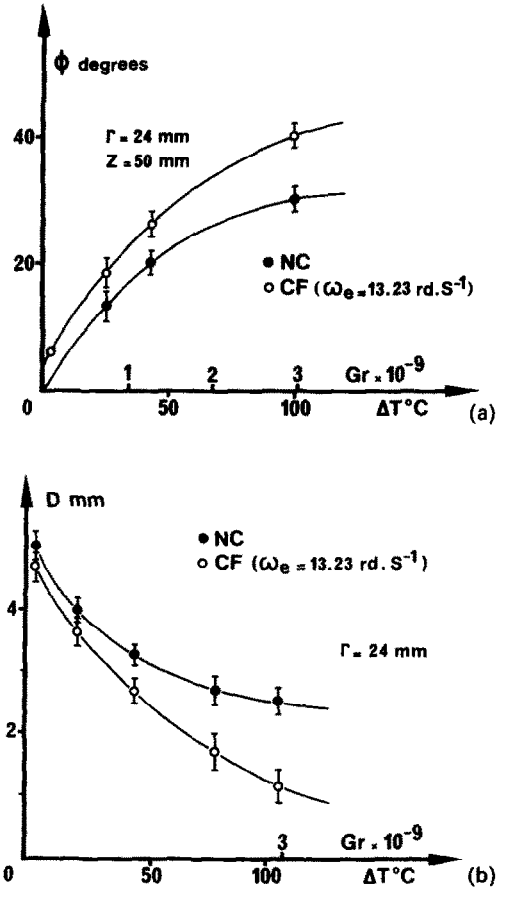


FIG. 14. Effect of the initial superheat (or of the initial Grashof number), in natural convection (NC) and in the presence of a forced Couette flow (CF): (a) on the angle of inclination $\phi$; (b) on the average diameter $D$ of the columns.

6.3. *Electromagnetic rotation*

Figure 13(e) conveys a typical example of directional solidification obtained in the presence of a magnetically driven rotating flow, provoked by application of crossed electric and magnetic fields. This macrography reveals the presence of fine blade-shaped crystals, once again inclined against the stream. Moreover, the columns grow horizontally confirming that, in this situation and contrary to the case of the Couette flow, the secondary loop, inside a radial cross-section of the melt, is virtually insignificant with respect to the movement of rotation. This finding is corroborated by observation of the sample depicted in Fig. 12(c), which exhibits the vertical sections of the blade-shaped columns. Although the columns are sloped counterflow, the mean velocity of the molten metal $U_m$ and the shear stress $\tau = \eta\, du/dr$ upon the interface of average radius $R_i$ affect the solute distribution, and hence act indirectly on the shape and size of the obtained crystals [28, 29]. So, the measurements of the angle of deflection $\phi$ (defined here with respect to a radius), made under the conditions of Fig. 13(e) and for different positions of the solidification front, have been connected with the measured corresponding hydrodynamic parameters. Inspection of Figs. 15(a) and (b) shows that $\phi$ first increases with $U_m$ and $\tau$, and then tends to a limit of about 50°. Attention must be drawn to the fact that a notable inclination of the dendrites can be obtained even for a relatively low mean velocity (or shear stress); e.g. $\phi \simeq 15°$, when $U_m = 1\ \mathrm{cm\,s^{-1}}$ (Fig. 15(a)). Methodical experiments have proven that, for a given initial superheat, the increase of the stirring intensity results in a decrease of the average diameter $D$ of the dendrites and in an enhancement of their inclination $\phi$. Likewise, it is seen in Figs. 15(c) and 16 that,

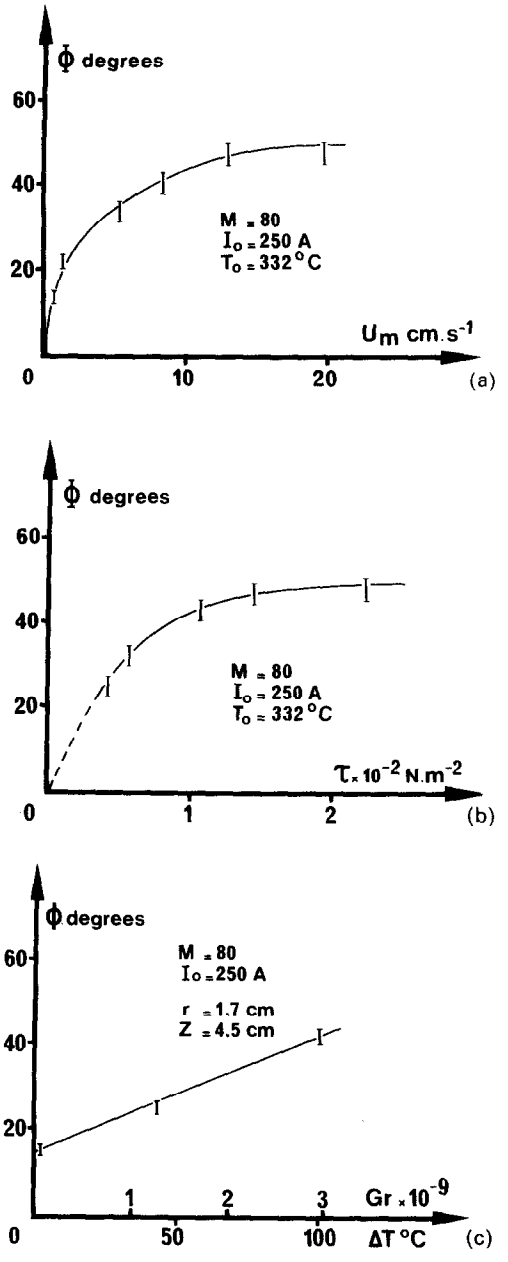


FIG. 15. Variation of the angle of deflection $\phi$ of the columnar crystals, in the presence of electromagnetic rotation, as a function of the average velocity (a), of the shear stress upon the interface (b) and of the initial superheat (c).

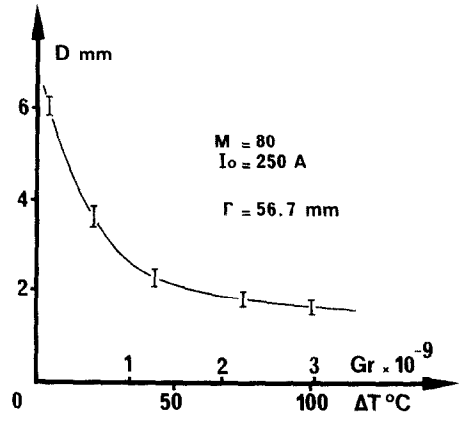


FIG. 16. Evolution of the average diameter of the columns, measured at a given radial position, as a function of the initial superheat, or of the initial Grashof number (electromagnetic rotation).

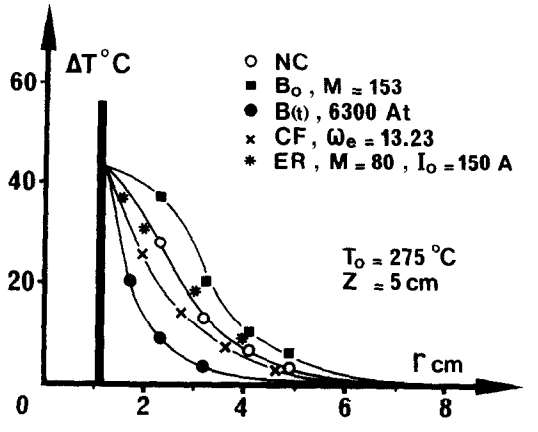


FIG. 17. Superheat drop as a function of the thickness of the solidifying crust in natural convection (NC), in damped convection ($B_0$) and in the presence of various forced convections, caused by an induction electromagnetic field ($B(t)$) by crossed and stationary electric and magnetic fields (ER) and by a forced Couette flow (CF).

all other stirring conditions remain unchanged, the curvature of the crystal increases and its thickness decreases, when superheat increases. On the other hand, the equiaxed structure which occurs (Fig. 13(c)) within a cortical area of about 1 cm thickness (connected with the latter stages of freezing, i.e. with a melt temperature close to the melting point (Fig. 17)), is coarser than that obtained in the presence of the Couette flow (Figs. 13(c) and (d)), because the shear stress is here much lower.

Figure 13(f) exhibits the effect of periodic reversals of the direction of the flow rotation obtained by inversion of the polarity of the electric current $I_0$ (every 150 s); the growing of zig-zag-shaped crystals is clearly revealed and, in accordance with the results displayed in Figs. 10 and 15(a), it may be seen that the value of $\phi$ is not significantly affected during the first three reversals of rotation.

## 7. CONCLUSIONS

The role of mixed convection, caused by mechanically, or electromagnetically, driven rotating flows during the solidification of tin in a toroidal mould, was investigated. The macrostructure of the solidified melt was examined and the metallurgical finding (crystal growth) connected with the heat and fluid flow

measurements. The deflection of columnar crystals has been particularly related to the mean velocity and the shear stress upon the melt–solid interface, as well as to the initial superheat. The dramatic effect of these various conditions of stirring on the shape and size of the directionally solidified crystals is pointed out in Figs. 12 and 13.

The results obtained here combine with a still more comprehensive and comparative study including investigations, reported in recent papers [10–17] and bearing on the solidification of a pure metal, either in the presence of natural convection [10, 17], or in the presence of time-varying [10] or stationary [17] magnetic fields. Figure 17 illustrates a representative example of the effects provoked by different situations of natural, forced and damped convection on the escape of superheat $\Delta T$ during solidification. The evolution of $\Delta T$ is particularly significant, on account of its repercussion on the solidification rate, as well as on the shape and size of the crystal. It is seen that, from the superheat drop standpoint, the stirring due to the application of an induction electromagnetic field [10] is more efficient than that produced by crossed and stationary electric and magnetic fields. Nevertheless, at the onset of freezing, the velocity peaks are of the order of 10 cm $s^{-1}$, in the first circumstance, and of 25 cm $s^{-1}$, in the second. In the case of the electromagnetic rotation, the velocity being mainly tangential does not contribute directly to adequate mixing. In contrast, in the presence of an induction electromagnetic field [10], the bulk liquid is rapidly homogenized, because the fluid particles, carried away by the recirculating vortex, travel alternately from a hot to a cold zone. Accordingly, it occurs that, in such a system, the flow structure is very important and that the stirring intensity (or the flow rate) is not the unique criterion of efficiency.

To summarize, these investigations have shown the spectacular impact of the flow patterns during the directional solidification of a pure metal. It is clearly evident that the application of electromagnetic fields of adequate pattern and strength is, in most cases, a very attractive method for the production of crystals of required shape and size, without pollution of the metal.

## REFERENCES


1. J. Szekely and P. S. Chhabra, The effect of natural convection on the shape and movement of the melt–solid interface in the controlled solidification of lead, *Metall. Trans.* **1,** 1195–1203 (1970).
2. J. Szekely, *Fluid Flow Phenomena in Metal Processing*, pp. 204–228. Academic Press, London (1979).
3. A. W. Hills, S. L. Malhotra and M. R. Moore, The solidification of pure metals (and eutectics) under unidirectional heat flow conditions: II. Solidification in the presence of superheat, *Metall. Trans.* **B6,** 131–142 (1975).
4. C. Gau and R. Viskanta, Melting solidification of a metal system in a rectangular cavity, *Int. J. Heat Mass Transfer* **27,** 113–123 (1984).
5. C. Gau and R. Viskanta, Effect of natural convection on solidification from above and melting from below of a pure metal, *Int. J. Heat Mass Transfer* **28,** 573–587 (1985).
6. H. S. Marr, Electromagnetic stirring: stepping stone to improved continuously cast products, *Iron Steel Int.* **2,** 29–41 (1979).
7. D. B. Spalding and N. H. Afgan, *Heat and Mass Transfer in Metallurgical Systems*. McGraw-Hill, New York (1981).
8. G. Abbaschian and S. David, Grain refinement in castings and welds, *Metall. Soc. A.I.M.E.* 3–63 (1983).
9. A. A. Tsavaras and H. D. Brody, Electromagnetic stirring and continuous casting—achievements, problems and goals, *J. Met.* **1,** 31–37 (1984).
10. Ch. Vivès and Ch. Perry, Effects of electromagnetic stirring during the controlled solidification of tin, *Int. J. Heat Mass Transfer* **29,** 21–33 (1986).
11. Ch. Vivès and B. Forest, CREM: a new casting process, Part 1: Fundamental aspect, light metals, *Metall. Soc. A.I.M.E.* 769–778 (1987).
12. K. H. Spitzer, M. Dubke and K. Schewerdtfeger, Rotational electromagnetic stirring in continuous casting of round strands, *Metall. Trans.* **B17,** 119–131 (1986).
13. D. B. Spencer, R. Mehrabian and M. C. Flemings, Rheological behavior of Sn-15 Pct Pb in the crystallization range, *Metall. Trans.* **3,** 1925–1932 (1972).
14. H. Kodoma, E. Nyama, M. Horiguchi, Y. Numata, T. Kimura et M. Endo, La solidification de billettes dans la lingotière d'une coulée continue de type rotatif synchronisé, *Revue Métall., C.I.T.* **6,** 521–533 (1983).
15. U. P. Utech and M. C. Flemings, Elimination of solute banding in indian antimonide crystals by growth in a magnetic field, *J. Appl. Phys.* **5,** 2021–2024 (1966).
16. D. R. Uhlmann, T. P. Seward and B. Chalmers, The effect of magnetic fields on the structure of metal alloy castings, *Trans. Metall. Soc.* **236,** 527–531 (1966).
17. Ch. Vivès and Ch. Perry, Effects of magnetically damped convection during the controlled solidification of metals and alloys, *Int. J. Heat Mass Transfer* **30,** 479–496 (1987).
18. M. Couette, Etudes sur le frottement des fluides, *Annls Chim. Phys.* **21,** 433–510 (1880).
19. A. Mallock, Determination of the viscosity of water, *Proc. R. Soc. London* **A45,** 126–132 (1888).
20. G. I. Taylor, Stability of a viscous liquid contained between rotating cylinders, *Phil. Trans. R. Soc. London* **A223,** 289–343 (1923).
21. G. Cognet, Les étapes vers la turbulence dans l'écoulement de Couette–Taylor entre cylindres co-axiaux, *J. Méc. Theorique Appliquée* numéro spécial, 7–44 (1984).
22. G. S. Hoppin and W. P. Danesi, Manufacturing processes for long-life gas turbines, *J. Metals* **38,** 20–23 (1987).
23. I. Minkoff, *Solidification and Cast Structure*, pp. 138–139. Wiley, New York (1986).
24. M. McLean, Directionally solidified materials for high temperature service, *Metals Soc.* (1983).
25. *Annual Book of A.S.T.M. Standards*, Section 3. American Society for Testing and Materials, Philadelphia (1983).
26. R. Ricou and Ch. Vivès, Local velocity and mass transfer measurements in molten metals using an incorporated magnet probe, *Int. J. Heat Mass Transfer* **25,** 1579–1588 (1982).
27. H. C. Lee, J. W. Evans and Ch. Vivès, Velocity measurement in Wood's metal using an incorporated magnet probe, *Metall. Trans.* **B4,** 734–736 (1984).
28. B. Chalmers, *Principle of Solidification*, pp. 270–276. Krieger, Malabar, Florida (1982).
29. T. Takahashi, K. Ichikawa, M. Kudou and K. Shimahara, The effect of fluid flow on the macrosegregation in steel ingot, *Trans. I.S.I.J., Japan* **16,** 283–291 (1976).

## EFFETS D'UN ECOULEMENT FORCE DE COUETTE PENDANT LA SOLIDIFICATION CONTROLEE D'UN METAL PUR

**Résumé**—On étudie le rôle de la convection mixte, provoquée par un écoulement de Couette, pendant la solidification dirigée de l'étain dans un moule toroïdal. La macrostructure du bain solidifié a été examinée et les résultats métalliques (croissance cristalline) ont été reliés aux mesures thermiques et hydrodynamiques. Les résultats ont été comparés avec ceux obtenus avec un autre type d'écoulement tournant, entraîné par un champ électromagnétique stationnaire produit par une pompe à conduction électromagnétique annulaire. L'angle de déflection des cristaux colonnaires a été particulièrement relié à la vitesse moyenne et au cisaillement sur l'interface liquide–solide, ainsi qu'à la surchauffe initiale.

## EINFLÜSSE EINER ERZWUNGENEN COUETTE-STRÖMUNG BEI DER KONTROLLIERTEN ERSTARRUNG VON REINEM METALL

**Zusammenfassung**—Der Einfluß der Mischkonvektion infolge einer erzwungenen Couette-Strömung bei der Erstarrung von Zinn in einer ringförmigen Gußform wurde untersucht. Die Makrostruktur der erstarrten Schmelze wird bestimmt und die metallurgischen Erkenntnisse (Kristallwachstum) mit den Messungen der Wärme- und Fluidströme in Verbindung gebracht. Die Ergebnisse werden mit andersartigen Rotationsströmungen verglichen, die durch ein stationäres elektromagnetisches Feld aufrechterhalten und durch eine elektromagnetische Pumpe erzeugt werden. Der Richtungswinkel der säulenförmigen Kristalle wird sowohl auf die mittlere Geschwindigkeit und die Schubspannung an der Grenzfläche der Schmelze als auch auf die anfängliche Überhitzung bezogen.

## ВЛЯНИЕ ВЫНУЖДЕННОГО ТЕЧЕНИЯ КУЭТТА НА ПРОЦЕСС РЕГУЛИРУЕМОГО ЗАТВЕРДЕВАНИЯ ЧИСТОГО МЕТАЛЛА

**Аннотация**—Исследуется роль смешанной конвекции, вызванной вынужденным течением Куэтта, в процессе направленного затвердевания олова в тороидальной пресс-форме. Анализируется макроструктура затвердевшего расплава, и полученные данные (о росте кристаллов) связываются с измерениями тепловых и динамических характеристик течения. Эти данные сравниваются с результатами исследования другого типа ротационного течения, вызванного стационарным электромагнитным полем, которое создается в кольцевом МГД-насосе. Угол изгиба кристаллов зависит от средней скорости течения и напряжения сдвига на границе раздела между расплавом и твердой фазой, а также от начального перегрева.